Missouri S&T Library and Learning Resources

Scholars' Mine

Masters Theses

Student Theses and Dissertations

Spring 2020

Strain partitioning across the Polochic-Motagua Fault System in Guatemala: Insight from kinematic modeling

Qiaoqi Sun

Follow this and additional works at: https://scholarsmine.mst.edu/masters_theses

 Part of the Geology Commons, and the Geophysics and Seismology Commons

Department:

Recommended Citation

Sun, Qiaoqi, "Strain partitioning across the Polochic-Motagua Fault System in Guatemala: Insight from kinematic modeling" (2020). *Masters Theses*. 8008.
https://scholarsmine.mst.edu/masters_theses/8008

This thesis is brought to you by Scholars' Mine, a service of the Missouri S&T Library and Learning Resources. This work is protected by U. S. Copyright Law. Unauthorized use including reproduction for redistribution requires the permission of the copyright holder. For more information, please contact scholarsmine@mst.edu.

STRAIN PARTITIONING ACROSS THE POLOCHIC-MOTAGUA FAULT SYSTEM IN GUATEMALA: INSIGHT FROM KINEMATIC MODELING

by

QIAOQI SUN

A THESIS

Presented to the Faculty of the Graduate School of the

MISSOURI UNIVERSITY OF SCIENCE AND TECHNOLOGY

In Partial Fulfillment of the Requirements for the Degree

MASTER OF SCIENCE IN GEOLOGY AND GEOPHYSICS

2020

Approved by:

Andreas Eckert, Advisor
Jonathan Obrist-Farner, Co-Advisor
John Patrick Hogan

© 2020

QIAOQI SUN

All Rights Reserved

ABSTRACT

The Polochic-Motagua Fault System in Guatemala is the on-land segment of the sinistral transform plate boundary between the North American Plate and the Caribbean Plate. Three major seismically active strike-slip faults in this fault system pose significant earthquake threats to surrounding populated cities. The assessment of seismic hazard requires a better understanding of the kinematics of the fault system. GPS monitoring indicates that seventy-five percent of the ~20 mm/yr. plate motion is accommodated by the Motagua Fault and less than twenty-five percent is accommodated by the Polochic Fault. However, the Polochic Fault documents a lateral offset of ~132 ± 5 km, forming a pull-apart basin and the introduction of more faults may change the strain partitioning. The 2D Finite Element Analysis is used to better constrain slip rates and improve established data. Previous kinematic models are not sufficient to provide the degree of strain partitioning due to interpreting the complex fault system as a singular structure.

In this study, we present new 2D finite element models of the fault network area in Guatemala to study strain partitioning of the plate boundary fault system. The preliminary model results are used to calibrate with published GPS data, resulting in a best-fit model. Such a model provides a better understanding of the structural geometry at the fault network and the strain distribution between different faults in the fault system. This modeling approach allows refinement of current structural models, and strain partitioning results will aid in future seismic hazard assessment in the fault system.

ACKNOWLEDGMENTS

I would like to thank my advisor, Dr. Andreas Eckert, for his careful guidance. He is an excellent mentor who always supports me and helps me with my studies. He encourages me to experience more academic events, such as poster presentations and oral presentations. Such things not only make me feel like I have gained lots of improvement during the master's degree, but also benefit me in my future studies, work and life.

I would like to express my gratitude to Dr. Obrist-Farner, who has given me the opportunity of this research. He is really an encouraging mentor and helps me a lot in my research and daily life. He is constantly motivating me to make greater progress in my studies and research.

I would like to thank Dr. Hogan for giving me academic guidance at the beginning of my master's degree. He offers lots of opportunities to experience American culture and participate in various activities, which is very important for me as an international student.

Thank you to everyone in the research group, Weicheng Zang, William Chandonia, Avery Welker, Chao Liu, Peter Nso, and Wenyu Zhao. They gave me a lot of help during my master's degree.

I would also like to thank my parents. They are celebrating with me when I succeed and are the best listeners when I am upset. They will offer all kinds of support when I encounter difficulties, and tell me home is my forever harbor.

Thanks to my roommates, Yutong Liu and Shiming Dong, for their support, understanding, and friendship. We are really lucky to know each other since the very beginning of the master's degree in the United States.

TABLE OF CONTENTS

Page

LIST OF ILLUSTRATIONS

Figure Page

LIST OF TABLES

1. INTRODUCTION

1.1. LITERATURE REVIEW

The Polochic-Motagua Fault System (PMFS) is in eastern Guatemala. The west-east trending PMFS is a sinistral plate boundary fault system that accommodates the motion between the North American Plate (NA) and the Caribbean Plate (CA).

1.1.1. Geological Setting. There are three roughly paralleled, strike-slip, left-lateral major faults included in the PMFS: the Polochic Fault (PF), the Motagua Fault (MF), and the Jocotan Fault (JOF) (Figure 1.1). The PF extends ~400 km on-land and experienced ~130 km offset (Burkart, 1978) in Neogene, forming a large pull-apart basin called the Izabal Basin that has a 4 km thickness of sediments (Lodolo et al., 2009). The MF extends ~ 300 km and experienced ~300 km Neogene displacements (Ratschbacher et al., 2009), creating the Motagua Valley which is covered by a 1 km thickness of sediments (Lodolo et al., 2009). The JOF is located on the southernmost side of the fault system and has a length of 200 km.

To the east, the PMFS is considered to connect with the Swan Fault (SF), which represents the plate boundary between the CA and NA in the Caribbean Sea, and then connects to the Cayman Trough (Lyon-Caen et al., 2006; Authemayou et al., 2012). At the west end of the PMFS, the Tonala Fault (TF) extends from the western tip of the PF towards the northwest and is roughly parallel to the west boundary of the CA. The Ixcan Fault (IF) is to the north and paralleled to the fault system. To the southwest of the PMFS, the plate boundary between the Caribbean Plate and the Cocos plate (CO) is marked by the Mid-American Trench (The NA, the CA, and the CO form a triple junction). This trench is

formed by the subduction of the CO beneath the overriding plates (the CA and the CO). This subduction zone induced the formation of a Volcanic Arc (VA). A rheologically weak zone, formed due to the VA, lies along the CA and results in the dextral strike-slip Jalpatagua Fault (JF).

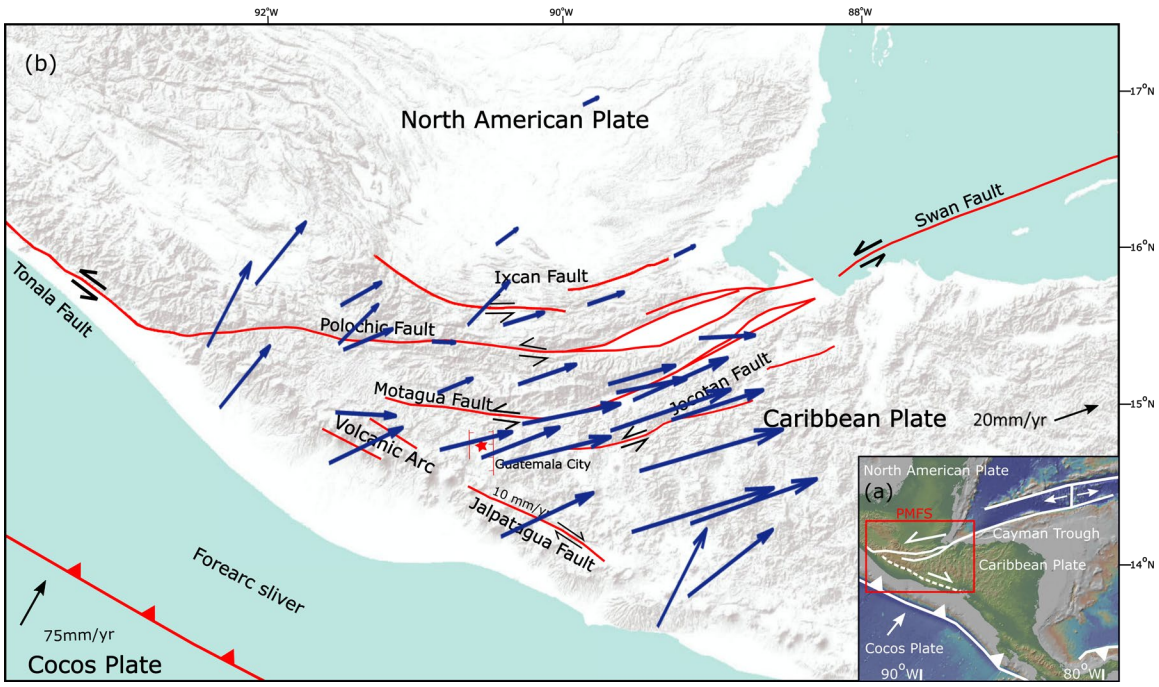

Figure 1.1 Tectonic setting of the PMFS (a) Plate tectonic setting of the Caribbean Plate. The red rectangular is the study area. (b) Tectonic setting and major faults (interpreted from the literature cited in 2.1 and highlighted with red lines) of the PMFS and adjacent area. Blue arrows are velocity vectors of GPS data from Franco et al. (2012).

1.1.2. Seismicity. The PMFS and adjacent area is a historically seismic area, including large active fault networks caused by the relative plate motion. Thus, the PMFS poses a significant earthquake hazard to surrounding populated cities (White, 1984). White (1984) studied the history of seismicity in the Guatemala region, including the epicenter of

earthquakes, magnitudes, and damages. For example, in 1785, an earthquake with M_w 7.3-7.5 ruptured the eastern part of the PF. In 1816, the western PF, adjacent to the location of the 1785 event, was ruptured by an earthquake with Mw 7.5-7.7 (White, 1984). The last destructive major earthquake occurred at the eastern MF in 1976 with a moment magnitude (M_w) of 7.5. This event ruptured the MF for over 230 km, which killed ~23,000 people and left 1.5 million people homeless (Plafker, 1976; Olcese et al., 1977). All of these events caused casualties and major damage to buildings. In addition, after the earthquake in 1976, Guatemala has tripled in population (worldbank, 2018); therefore, the next major seismic event in this fault network could be even more devastating.

1.2. OTHER STRIKE-SLIP FAULTS

Plenty of other large active strike-slip plate boundary fault systems on earth have experienced severe seismic activities. Recent major earthquakes on the San Andreas Fault (SAF) in California include the Mw 7.3 Landers earthquake in 1992 (Hauksson et al., 1993), the Mw 7.1 Hector Mine earthquake in 1999 (Fialko & Simons, 2001; Fialko et al., 2002), and the 2019 Mw 7.1 Ridgecrest earthquake (USGS.gov, 2019). Many seismic events have been reported on the North Anatolian Fault (NAF) in Turkey, such as the 1939 Erzincan earthquake with Mw 7.9, the 1943 Tosya earthquake with Mw 7.6, and the Bolu-Gerede earthquake in 1944 with Mw 7.6 (Ambraseys, 1970; Barka, 1996). Along the Alpine Fault (AF) in New Zealand, major seismic events include 1717 Mw 7.9 earthquake (De Pascale & Langridge, 2012), 1620 Mw 7.6 earthquake, and 1430 Mw 7.9 earthquake (Sutherland et al., 2007). Large earthquakes on plate boundary fault systems also include the 1995 Nuweiba earthquake in the Dead Sea Fault (DSF) that ruptured the southern

section with M_W 7.1 (Baer et al., 1999). Each of those seismic events experienced ruptured faults for hundreds of kilometers and caused damage to adjacent cities.

Conclusions from studies on other strike-slip faults, earthquake nucleation, propagation, and termination along strike-slip plate boundary faults are dependent on how strain is accumulated and partitioned across the often-multiple fault branches of such fault systems. As high stress accumulation has the potential to trigger large earthquakes, the degree of strain partitioning will indicate where the next event is more likely to strike.

One example is the San Andreas Fault (SAF), which released large amounts of previously accumulated strain that triggered the Hector Mine earthquake and ruptured the preexisting faults (Fialko & Simons, 2001; Fialko et al., 2002). In addition, the strain could also possibly be released to surrounding faults, leading to a new rupture (Barka, 1996; Stein et al., 1997). For example, earthquakes transferred along the North Anatolian Fault system (NAF) from east to west due to the stress release (Hussain et al., 2016; Barka, 1992, 1996). Therefore, understanding the accumulation and partitioning of strain is one key to understanding seismic hazards.

Different methods have been used to study the kinematics of plate boundary fault systems to understand strain partitioning. These methods include trenching (Lefevre et al., 2018; Wechsler et al., 2018; McGill et al., 2002), Global Positioning System (GPS) measurements, and Interferometric Synthetic Aperture Radar (InSAR) (Lindsey and Fialko, 2013; Lindsey et al., 2014; Tymofyeyeva & Fialko, 2018; Szeliga et al., 2012). Based on these methods, certain large strike-slip plate boundary fault systems have been thoroughly studied to investigate the possibility of future seismic events. The SAF is a complex plate boundary fault system with fast relative motion of ~40 mm/yr (Bennett et

al., 1996). Recent studies mainly focus on the southern part of the SAF. Due to the continued strain accumulation that occurs when there are no seismic events in hundreds of years, the SAF presents a large possibility to trigger major earthquakes (Lindsey & Fialko, 2013; Tymofyeyeva & Fialko, 2018; Lindsey et al., 2014; Fialko, 2006). The NAF is characterized by westward decreasing slip rates (Hussain et al., 2016; Barka, 1996, 1992). Since the geometry is simple without many adjacent fault segments, all strain should be constrained on the main fault trace. This results in the stress accumulation that builds in the near part of the failure segments, which is considered to be the location of future earthquakes (Barka, 1996; Stein et al., 1997). The Dead Sea Fault (DSF) has a relatively slow motion of ~4 mm/yr (Wdowinski et al., 2004). However, the long quiescence from large ruptures indicates that the fault system has already accumulated a large amount of strain and is prepared to rupture, especially in the southern part of the DSF and the Yammouneh Fault (bounded a restraining bend) (Wechsler et al., 2018; Hamiel et al., 2018; Lefevre et al., 2018; Gomez et al., 2007). The total motion accommodated on the Alpine Fault (AF) is about 27±5 mm/yr, and the maximum velocity is in the central South Island. The highest strain of this fault system is currently partitioned on the Hope Fault to the north (Langridge et al., 2010; Norris & Cooper, 2001; Sutherland et al., 2007). All these strain studies are helpful to understand the evolution of the fault system and future earthquakes.

1.3. RESEARCH OBJECTIVES AND QUESTIONS

Like other large plate boundary strike-slip fault systems, destructive earthquakes have been historically widely distributed in our study area. Following previous studies of other major strike-slip fault systems, the method to understand the kinematic should be

used to study within the PMFS.

1.3.1. Objectives. This study simulates the kinematics of the PMFS by using 2D Finite Element Analysis. The main objective of this study is to:

- Refine the strain partitioning across the PMFS.
- Improve the understanding of the kinematic of the fault system.

1.3.2. Previous Studies of Kinematic and Modeling of the PMFS. From the GPS measurements, some current kinematic information has been revealed. The far-field velocity of the PMFS has been decreasing from 20 mm/yr in eastern Guatemala to several mm per year at offshore southwestern Mexico (Lyon-Caen et al., 2006; Franco et al., 2012). The velocity continues to decrease to ~0 mm/yr at TF. Previous studies indicate that within the PMFS, the PF only accommodates 25% (~5 mm/yr) of the total 20 mm/yr plate boundary motion and about 75% (Lyon-Caen et al., 2006; Authemayou et al., 2012) or 65% (Ellis et al., 2019) remains on the MF. Along the Mid-American Trench, the subduction of the CO is at a velocity of 70-80 mm/yr (DeMets, 2001; Ellis et al., 2019). The JF lies on the VA, accommodating the motion from the retreating CA, with a velocity of 10 mm/yr (Lyon-Caen et al., 2006). However, the GPS measurements have their shortcomings. Many GPS sites do not include continuous GPS measurements. GPS campaigns record data in a short period of time, and are usually affected by many situations, and they cannot tell if this period is a seismic period or interseismic period, which may cause errors.

There are already several studies using the finite element method to simulate the geometry of this area in order to perform kinematic investigations. Alvarez-Gomez et al. (2008) and Rodriguez et al. (2009) indicate that the Volcanic Arc (VA) is a weak zone that

is about one magnitude of Young's Modulus lower than surrounding areas. In addition, the subduction of the CO is characterized as low coupling, which means that less strain is transferred from the CO to the overriding plates. These model results are consistent with information provided by Lyon-Caen et al. (2006) and Franco et al. (2012). The PMFS in those models are modeled as a singular structure.

1.3.3. Questions. Despite doing all these kinematic studies, including model simulation, some questions still remain. For example, the smooth curve of velocity profiles across the PMFS created with GPS data (Lyon-Caen et al., 2006; Franco et al., 2012) does not provide sufficient details of the degree of strain partitioning over the plate boundary fault system. Furthermore, not enough faults have been included in previous studies. In addition, the GPS campaign may not be reliable, and the PMFS in these studies is treated as a homogenous fault zone. However, the strain should be partitioned unevenly on each fault, which results in various earthquakes. The strain distribution is also connected with structure geometry (Rodriguez et al., 2009; Alvarez-Gomez et al., 2008), while some unknowns remain about structure geometry due to difficulties like vegetative covered surfaces and less geodetic data.

Research questions to be addressed:

- What is the influence of the geometry on the degree of strain partitioning?
- Which fault is connected to the Swan Fault?
- Is the Jocotan fault an active fault of the plate boundary?
- What is the influence of the friction coefficient on the faults?
- How much strain is laterally transferred across the subduction zone?
- What is the relative role of each of the faults as part of the plate boundary?

2. METHOD

This study simulates the Polochic-Motagua Fault System in Guatemala by using the 2D Finite Element Method to derive the degree of strain partitioning of each fault. In order to get the best model results, the geometry must be initially tested. The 2D linear elastic model is utilized to fill the knowledge gaps in strain partitioning, and fault system geometry which includes fault connections, presence of weak zones, and low coupling. This model is built via the Altair Hypermesh with the slip rate results being calculated by the software package Abaqus™.

The finite element method is useful in improving data from previous studies, particularly if the comprehensive geodetic data are not available (Nabavi et al., 2018).

In this study, we use 2D finite element modeling to analyze the different roles of faults by testing the structure geometry and simulating the PMFS and the surrounding areas. We test several scenarios and calibrate the results with GPS data (Lyon-Caen et al., 2006; Franco et al., 2012). The model results accurately reflect the GPS data such that the steps of velocity change across each fault in the fault system shows the degree of strain partitioning on each fault.

2.1. MODEL SETUP (GEOMETRY AND BOUNDARY CONDITIONS)

This model is a 2D plane stress linear elastic model georeferenced in WGS 1984 UTM Zone 16N projected Coordinate System. The rectangular model, with a size ~600 km × 700 km, covers major faults network area. Triangular elements are mainly used to fit the corners. This 2D plane stress kinematic finite element analysis model comprises two plates,

the North American Plate and the Caribbean Plate. The Polochic-Motagua Fault System, which separates the two plates, includes three major strike-slip faults (the PF, MF, and JOF). The Swan Fault and Tonala Fault are located on the east and west side of the fault system. The right lateral Jalpatagua Fault is included within the Caribbean Plate and is relatively parallel to the model boundary. All geometries in this model follow previously published geological maps and consider historical seismicity distributions (Franco et al., 2012; Lyon-Caen et al., 2006; Authemayou et al., 2012; Bartole et al., 2019; Ellis et al., 2018). All faults are introduced as constantly moving frictional interfaces with a coefficient of friction of 0.6.

Boundary conditions: as shown in Figure 2.1, black solid triangles represent fixed edges, black arrows represent moving edges, and rollers represent nodes that are fixed in the direction perpendicular to the edge and are free in the direction parallel to the edge. The velocity used for the CA is 20 mm/yr, and the orientation is 069˚. The CO has a velocity perpendicular to the trench of 75 mm/yr (Ellis et al., 2019).

In this model, the far-field strain is modeled by fixing the North American Plate and dragging the Caribbean Plate to the east-northeast, in order to compare the slip differences between two plates and derive slip rates of each fault within the PMFS. The south-west edge of this model represents the subduction zone between the CO and the two overriding plates. Therefore, even excluding the CO, this model still applies the strain that transferred from the CO to the overriding plates. This model also includes 33 GPS sites and 3 velocity profiles, shown in Figure 2.2, to help compare the model results with GPS data.

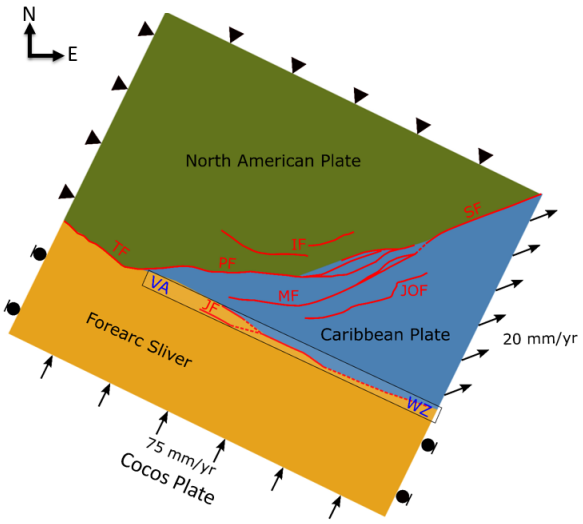

Figure 2.1 The sketch of model geometries and boundary conditions. Black triangles represent the fixing edge. Red abbreviations are for faults, TF: Tonala Fault, PF: Polochic Fault, MF: Motagua Fault, SF: Swan Fault, JOF: Jocotan Fault, JF: Jalpatagua Fault. The r is the location of the weak zone along the volcanic arc, VA: Volcanic Arc, WZ: Weak Zone. Red lines are highlights of faults. Dashed lines represent the tested connection of geometries.

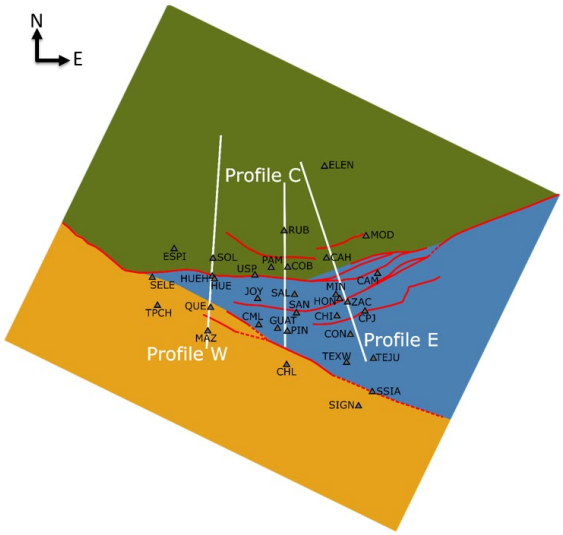

Figure 2.2 Model with GPS sites and velocity profiles. Locations of 33 GPS data sites (grey triangles) and 3 velocity profiles (white lines) in the model following Lyon-Caen et al. (2006) and Franco et al. (2012).

2.2. PROPERTIES

The elastic parameters include the Young's Modulus, the Poisson's Ratio, the friction coefficient, and the coupling (Correa-Mora et al., 2009) of the subduction zone. (Table 2.1) The values for Young's Modulus and Poisson's ratio follow Alvarez-Gomez et al. (2008) and Rodriguez et al. (2009) and represent the rheology of general rocks. The friction coefficient of faults is 0.6 (Byerlee, 1978). The coupling of the subduction zone uses 0.6-0.25 (Franco et al., 2012) for the base model to represent moderate to low strain transferred from the CO to the overriding plates.

Without detailed geometry measurements and testing in this area, some information is needed to improve the models. The friction coefficient is tested with 0.6 (high friction) and 0.1 (low friction) to simulate strong vs weak faults. The coupling of subduction is tested from 0 to 0.6 based on Franco et al. (2012). A weak zone has been predicted parallel to the trench along the Jalpatagua fault due to the underground magma flow (Rosenberg & Handy, 2005; Alonso-Henar et al., 2015; Garibaldi et al., 2016), which is characterized by a Young's Modulus one order of magnitude lower than surrounding areas (Alvarez-Gomez et al., 2008; Rodriguez et al., 2009). The test of geometry also includes the connection, activity, and position of faults (detailed explanation in the next section).

All model results are calibrated with the GPS data from Lyon-Caen et al. (2006) and Franco et al (2012).

Table 2.1 Model scenarios investigated in the simulation.

Parameters	Model	The connection between the PMFS and SF	The coupling of subduction	The geometry of JF	The JOF activities	Frictional Coefficient
Basic	1	No connection	0.6-0.25	Fault segments	Inactive	All 0.6
Connection between the PMFS and SF	2	PF-SF	0.6-0.25	Fault segments	Inactive	All 0.6
	3	MF-SF	0.6-0.25	Fault segments	Inactive	All 0.6
The coupling of subduction	4	MF-SF	0.4-0.15	Fault segments	Inactive	All 0.6
The geometry of the JF	5	MF-SF	0.4-0.15	Through-going JF	Inactive	All 0.6
JOF activities	6	MF-SF	0.4-0.15	Through-going JF	Active	All 0.6
Friction Coefficient	7	MF-SF	0.4-0.15	Through-going JF	Active	0.6 (JF 0.1)

3. RESULTS

All modeling results will be described in the following content and test the following scenarios: the connection between the PMFS and the SF, the activity of the JOF, the length of the JF, the friction coefficient of faults, and the coupling of the subduction zone.

To compare the model results with GPS data, we use two kinds of plots; the fault parallel motion plots which extract model results along three velocity profiles: profile E, C, and W, same as previous studies by Lyon-Caen et al. (2006) and Franco et al. (2012), and the vector plot of 33 locations at GPS sites.

For fault parallel motion plots, the X-axis is horizontal distance and Y-axis represents fault parallel motion. The location of faults is demonstrated in the figure by colored vertical lines. The pink line is the position of the IF, the blue line represents the position of the PF, the yellow line represents the MF, the purple line represents the JOF, and the green line represents the JF. Dark blue points are GPS data from Franco et al. (2012). The stepped line is the model result of velocity change across the fault system, and the circles are model results of GPS sets. In addition, we use ELEN as the reference point to compare the GPS data with model results. For vector plots, the blue arrows are GPS data from Franco et al. (2012).

3.1. INITIAL MODEL

The first model is only based on the map that was decided by several published geological maps, seismicity distribution, and previous study results. The PMFS remains

unconnected with the SF, and the JOF is inactive. The JF includes three segments that are directly analyzed from geological maps. The friction coefficient of faults uses 0.6, and the coupling of the subduction zone is 0.6-0.25 from west to east based on Franco et al. (2012).

3.1.1. Profile E. Profile E shows the velocity change across the fault system in eastern Guatemala (Figure 3.1). The total motion between the NA and the CA is ~ 14.5 mm/yr, and the stepped line shows the strain partitioned on each fault. The slip rates are 2 mm/yr, 5 mm/yr, 5 mm/yr, and 0 mm/yr on the IF, PF (two branches), MF, and JOF respectively. The GPS data and model results match with each other to the north of the JOF, while not enough strain is released on the CA plate.

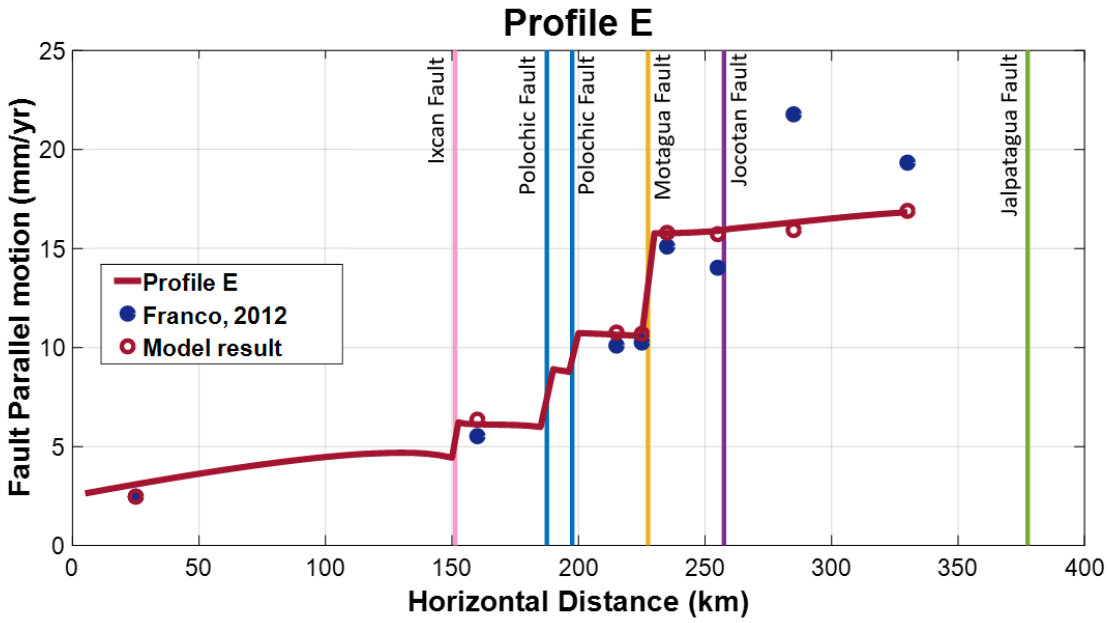

Figure 3.1 The model results of velocity change along profile E based on the original model.

3.1.2. Profile C. Figure 3.2 shows the degree of strain partitioning on each fault along Profile C in central Guatemala. Based on the step line, 2 mm/yr, 3 mm/yr, and 2 mm/yr slip rate occurred on the IF, PF, and MF respectively. The model results accurately match the GPS data to the north of the MF, while the strain released on the CA is small. The total motion for the model is ~9 mm/yr while the GPS shows ~13 mm/yr relative motion. The data line bend at the western end between the MF and the JF is due to the influence of the weak zone.

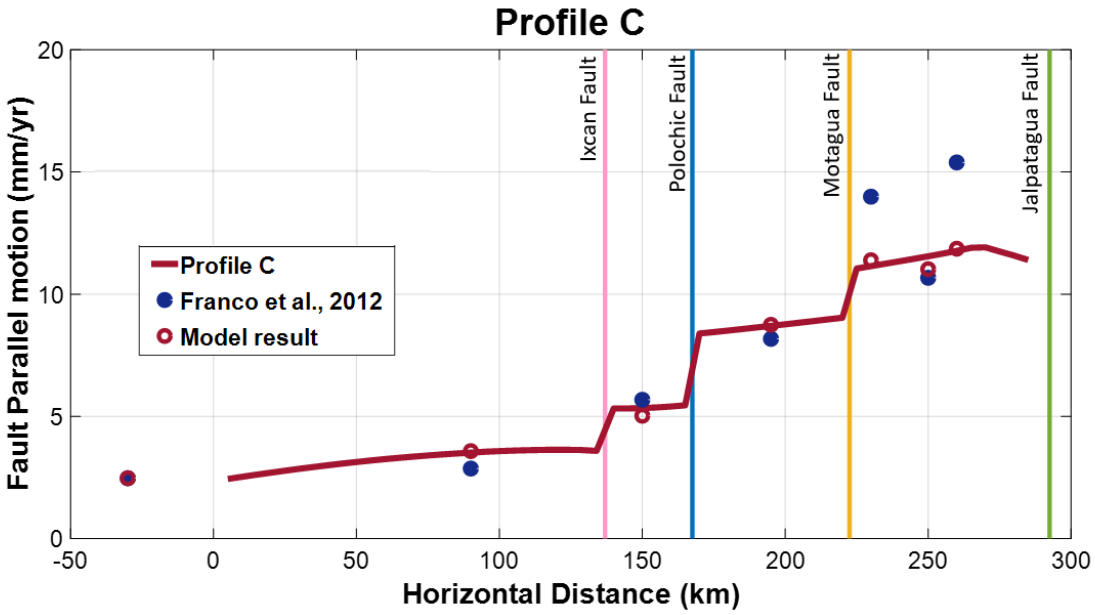

Figure 3.2 The model results of velocity change along profile C based on the original model.

3.1.3. Profile W. The step line shows the degree of strain partitioning on each fault along profile W in western Guatemala (Figure 3.3). The slip rate is about 3 mm/yr on the PF and ~ 0.2 mm/yr on the southern branch of the JF. Total motion is ~ 7 mm/yr. While

the GPS data and model results only partially match each other, the sites HUEH and HUE have 2-3 mm/yr difference, and ~1 mm/yr off at site MAZ. The bends around the JF are due to the influence of the weak zone.

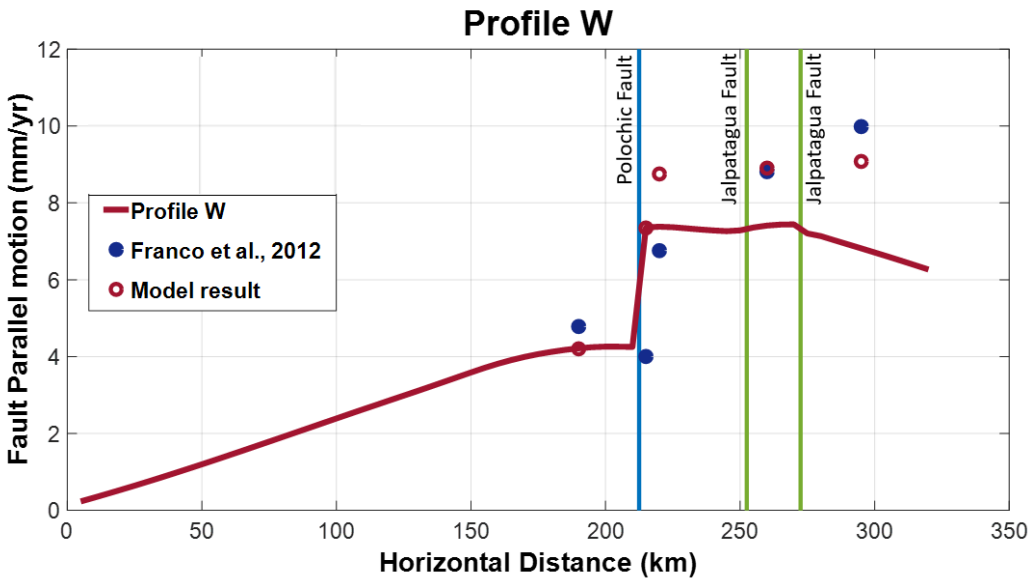

Figure 3.3 The model results of velocity change along profile W based on the original model.

3.1.4. Vector Plot. Red vectors are from model results (Figure 3.4). Overall, the model vector and GPS vector are roughly at the same orientation and magnitude. More in-depth inspection reveals that the model results are double in magnitude than GPS at the western part (around Profile W), whereas smaller in the CA (CON, TEXW). In addition, the orientations of the sites are all slightly shifted to the north, especially sites QUE, MAZ, and CHL.

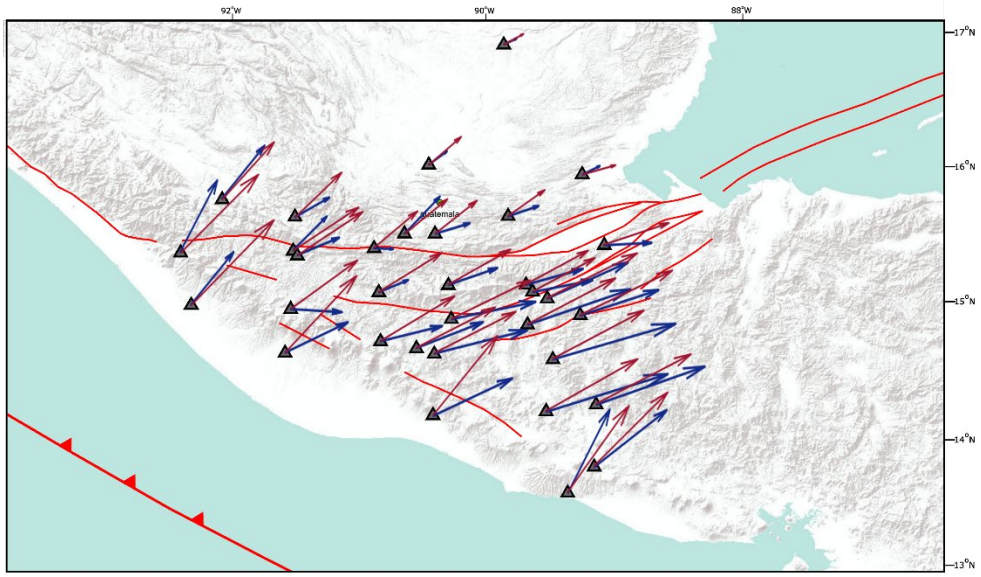

Figure 3.4 The vector plot based on the original model.

Based on the fault parallel motion and vector plots from the original model, the results are not perfectly consistent with the GPS data. The origin model should be improved by filling knowledge gaps.

3.2. CONNECTION TESTING

The connection between the PMFS and the SF remains unknown based on previous studies. In this model, we tested the connection: connect the PF or MF with SF. Figure 3.5 shows the different strain partitioning on faults along profile E. From the results, the grey line perfectly matches with GPS data to the north of the MF. Between the MF and the JOF, three models are all slightly higher than expected, while to the south of the JOF, model data are 2-5 mm/yr smaller than GPS. Figure 3.6 and 3.7 shows different strain partitioning on faults along profile C and W. The velocity differences between models are all within 1

mm/yr. To the north of the MF, GPS data and model results match each other while in the CA plate, model results are smaller than GPS data. From Figure 3.8, west Guatemala experienced an excess of strain in the model compared to the GPS data. On the CA, vectors from models did not obtain enough strain from CA plate retreat and accommodate too much strain from subduction of CO. From different connections between the PMFS and the SF, results show difference only around east Guatemala, the grey vector matches the GPS data better.

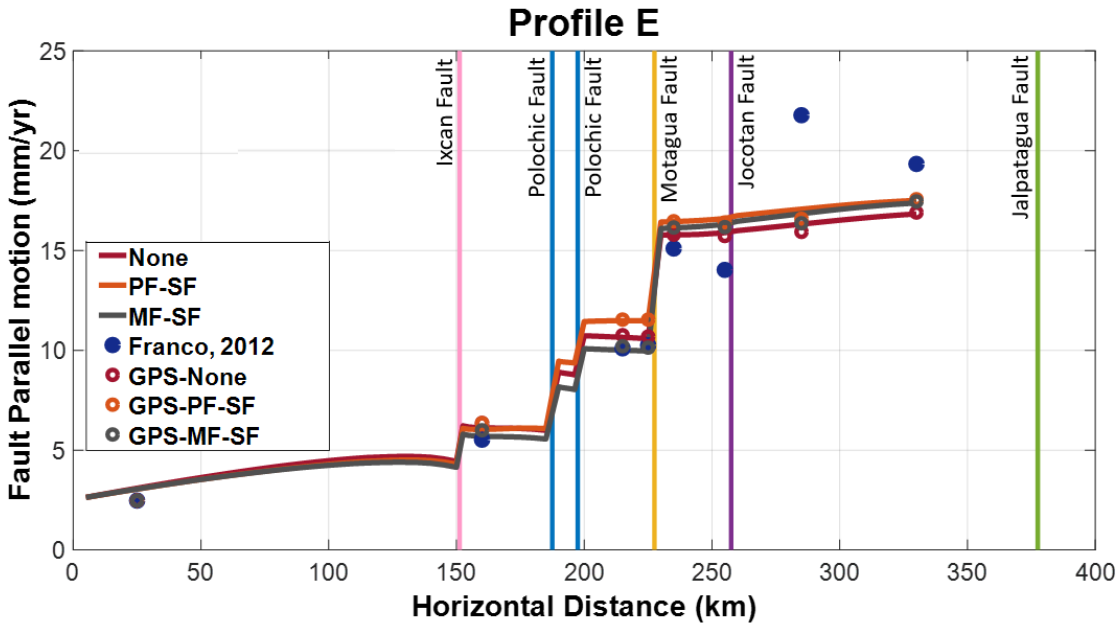

Figure 3.5 The model results of velocity change along profile E based on different connections between the PMFS and the SF. The grey line, dark red line, and orange line represent no connection between the PMFS and the PF, connect the PMFS with the PF, and connect the PMFS with the MF respectively.

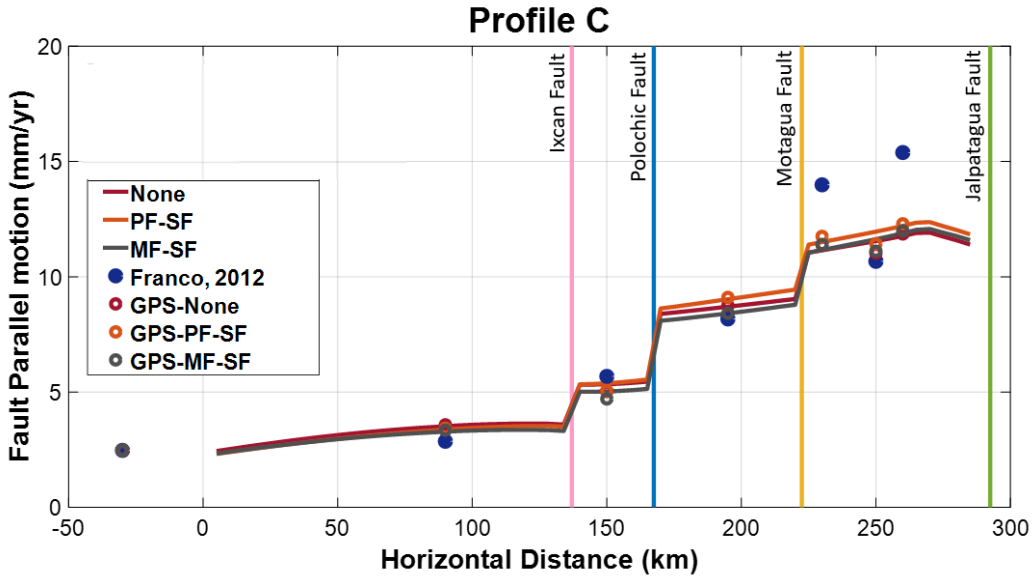

Figure 3.6 The model results of velocity change along profile C based on different connections between the PMFS and the SF. The grey line, dark red line, and orange line represent no connection between the PMFS and the PF, connect the PMFS with the PF, and connect the PMFS with the MF respectively.

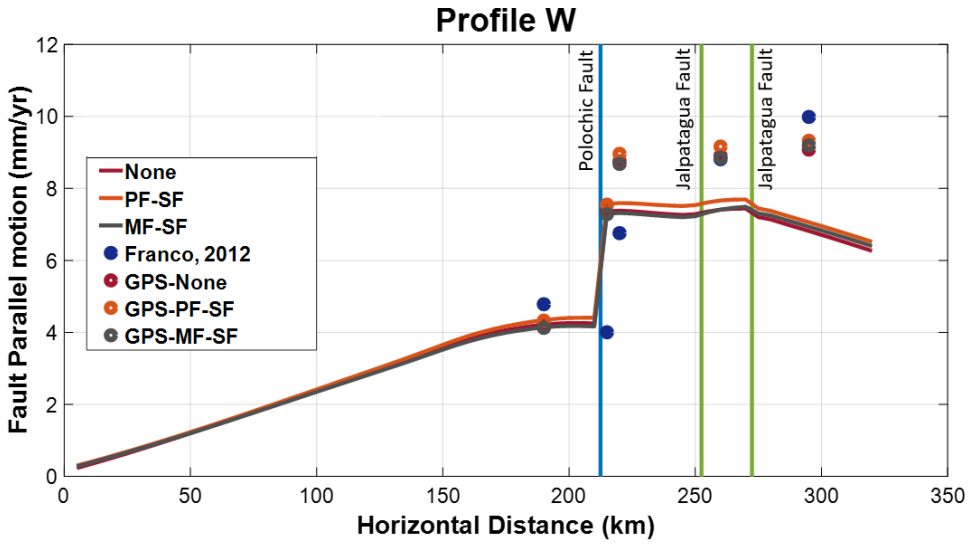

Figure 3.7 The model results of velocity change along profile W based on different connections between the PMFS and the SF. The grey line, dark red line, and orange line represent no connection between the PMFS and the PF, connect the PMFS with the PF, and connect the PMFS with the MF respectively.

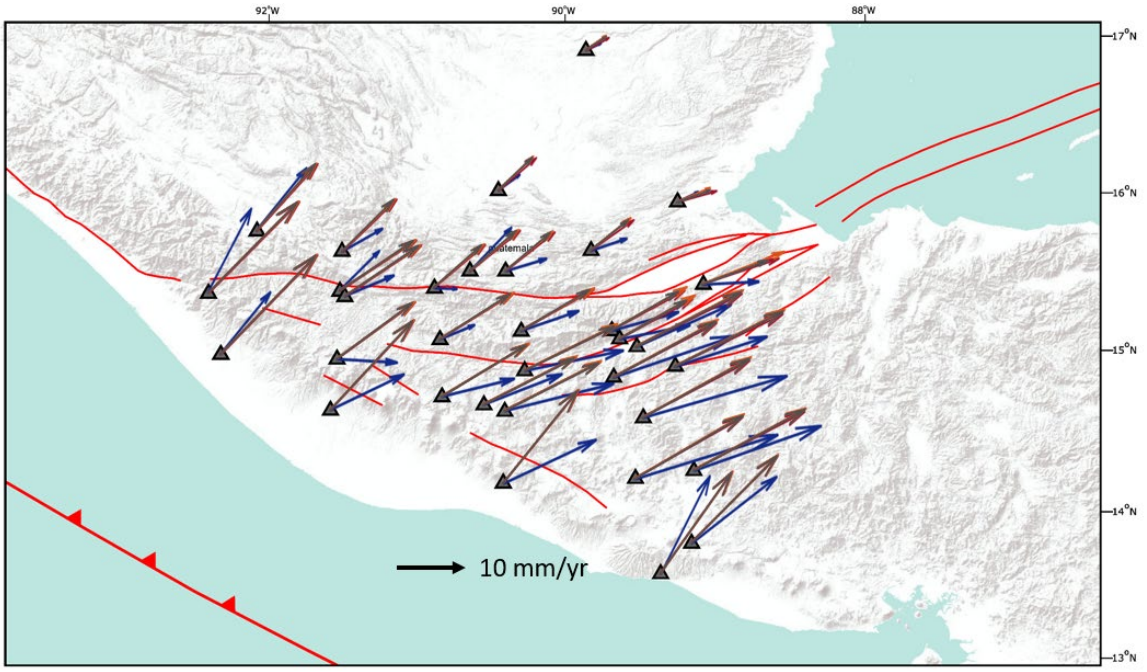

Figure 3.8 The vector plot of model results and GPS data based on models with different connections between the PMFS and the SF. The blue arrows are GPS data from Franco et al. (2012). The grey, dark red, and orange arrows represent no connection between the PMFS and the PF, connect the PMFS with the PF, and connect the PMFS with the MF respectively.

3.3. COUPLING OF CO SUBDUCTION

The most obvious difference between the model results and the GPS data is shown in the vector map. Figure3.9 shows that the previous model results experienced large amounts of strain transferred across the subduction zone, especially in western Guatemala (grey arrows). The coupling that is given in Franco et al. (2012) is calculated by GPS velocity inversion, with an uncertainty that the locking depth is assumed to be 25 km. Based on the inversion result with uncertainty, we decreased the coupling value at the west side, where it appears highly inconsistent with GPS data. Figure 3.9 shows the vector change

when the coupling is decreased along the subduction zone. Therefore, after reducing the coupling, the model results are more consistent with the GPS data.

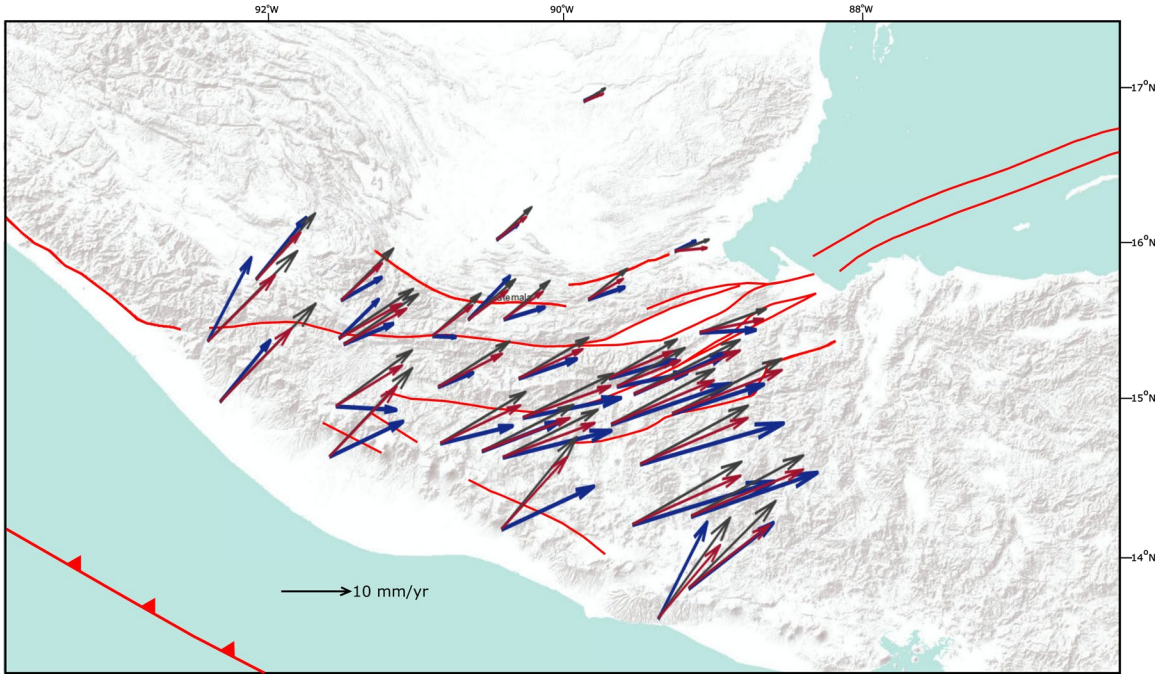

Figure 3.9 The vector plot of model results and GPS data based on models with different degree of coupling along the subduction zone. The blue arrows are GPS data from Franco et al. (2012). The grey and dark red arrows represent a model with origin coupling from Franco et al. (2012) and decreased coupling based on the same trend respectively.

3.4. JF EXTENSION TEST

The dextral motion of the JF is 10-14 mm/yr (Lyon-Caen et al., 2006; Franco et al., 2012). From the model slip result, the JF is currently accommodated only 5 mm/yr. Therefore, we extend the JF to both sides and connect segments together (Authemayou et al., 2012). The position and length of the extended JF are shown in Figure 3.10, with a dextral slip rate of ~12 mm/yr. After extending the JF, the vector plot does not change

much on the NA plate, vectors on the CA rotate slightly to the south and better fit the GPS data. The east part of the JF experienced major change after extending the JF, the SIGN, and SSIA accommodate less strain from the CA.

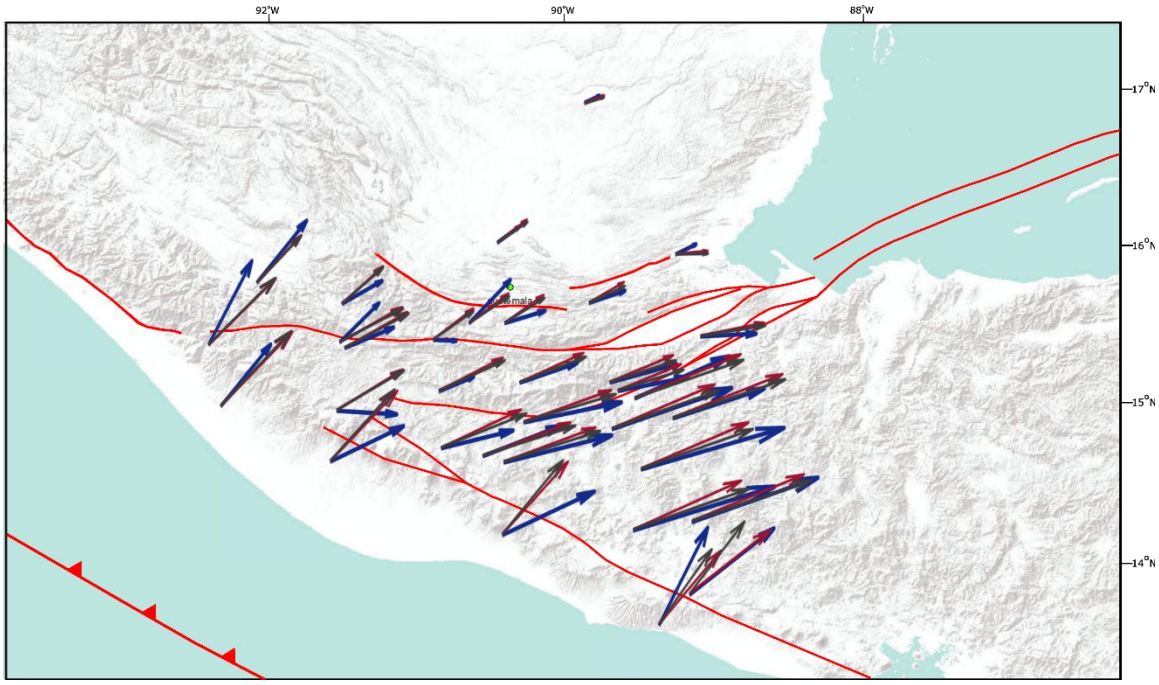

Figure 3.10 The vector plot of model results and GPS data based on models with different JF geometry. The blue arrows are GPS data from Franco et al. (2012). The grey and dark red arrows represent a model with extended JF and without extended JF respectively.

3.5. JOF ACTIVITY TEST

There are only one of the three velocity profiles across the JOF. From the result of profile E (Figure 3.11), the JOF accommodated a ~2 mm/yr slip rate. The GPS data shows that the site CPJ and CON have over 7 mm/yr slip which means there should be some slip experienced on the JOF.

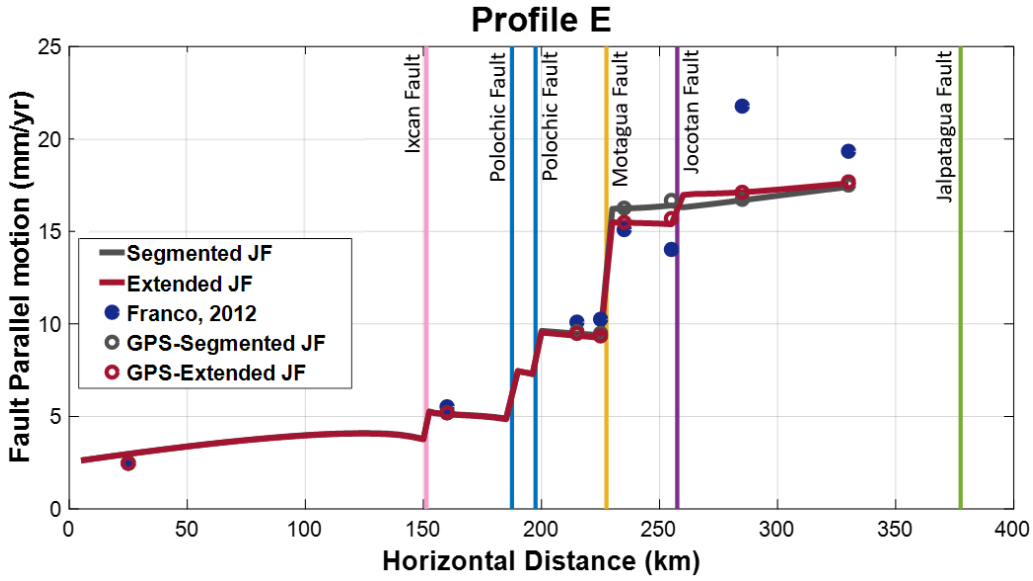

Figure 3.11 The model results of velocity change along profile E based on models that with or without the JOF. The grey line and dark red line represent inactive JOF and active JOF respectively.

3.6. FRICTION COEFFICIENT TEST

One property that has a major effect on faults is the friction coefficient which has not been tested in previous studies. Faults could become weak due to the lithology of the contact surface and the present of fault gouge (Dengo & Logan, 1981; Lavallee et al., 2014; Carpenter et al., 2015), etc. Based on current results, we tested a low friction coefficient for each fault.

The JF is along the volcanic arc; the volcanic arc could affect the behavior of fault. We apply 0.1 instead of 0.6 for the JF to test the possibility of a low friction coefficient. Figure 3.12 shows vector changing when varying the friction. From this figure, there is not a significant change, while vectors match the GPS data better.

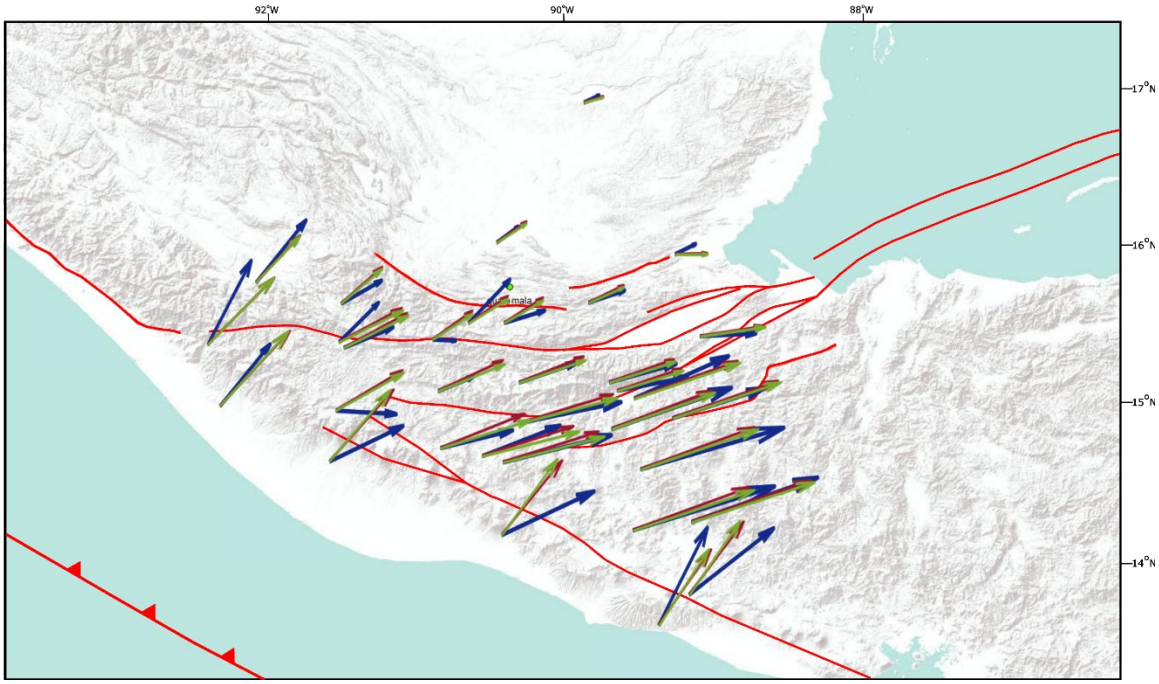

Figure 3.12 The vector plot of model results and GPS data based on models with different friction coefficient. The blue arrows are GPS data from Franco et al. (2012). The green and dark red arrows represent models with the JF friction coefficient 0.1 and 0.6 respectively.

4. DISCUSSION

Various kinematic studies show that strain partitioning is the key point to understand fault behavior and seismic hazard. In this study, 2D finite element modeling is used to determine the degree of strain partitioning for the PMFS by testing the control properties and geometries. From the comparison of model results, the best-fit model is derived. This model connects the Motagua Fault with the Swan Fault, is applying 40-15% of lateral coupling across the Mid-American Trench from west to east, includes the currently active Jocotan Fault, includes the through-going Jalpatagua Fault, and is applying 0.6 friction for fault interfaces with a low friction coefficient (0.1) for the JF.

4.1. LIMITATIONS OF THE MODELING APPROACH

This study using the 2D Finite Element Model to help to test some knowledge gaps of the fault geometries and to understand the strain partitioning across the PMFS. However, due to the less availability of reliable data, this modeling approach has limitations.

One limitation is the uncertainty of the geometry of the fault system. Fault traces of this model are derived from previous published geological maps, while, none of them did detailed mapping of those faults. Therefore, although we have carefully selected the faults that we used in the model, the uncertainty of the fault line itself has created limitations.

The lacking of experiment data of rock properties causes limitations. Some properties, for example, the friction coefficient and Young's modulus, that applied on the faults are from previous studies (Byerlee, 1978; Alvarez-Gomez et al., 2008; Rodriguez et

al., 2009). Although these data have shown their value in previous papers, they are untested and remain uncertain.

The 2D model also has limitation itself. For example, the 2D model cannot simulate the grabens in this area. The grabens, which represent the block extension, distributed at the wedge of the CA. The extension of those grabens will introduce more strain in those areas and release more movements, which could affect the strain partitioning in the fault system area.

In addition, the 2D model simulate long-term slip-rate instead of interseismic slip-rate, which recorded by GPS measurements. The meaning of using time-averaged geological slip-rate is to show how is the strain partitioned on each fault. Geological slip-rate equals interseismic slip-rate plus coseismic slip-rate.

4.2. THE ROLE OF EACH FAULT IN THE PMFS

The velocity profiles of the best-fit model shown in Figures 4.1, 4.2 and 4.3 are comparing with the results of previous studies to demonstrate the degree of strain partitioning. Many of the results are consistent with previous studies. The degree of strain partitioned on northern PF on Profile E, main PF on Profile C and Profile W are all 3 mm/yr. This result agrees with Ellis et al. (2019) that ~3.2 mm/yr for the PF, while slightly smaller than geological result 4.8 mm/yr (Authemayou et al., 2012). The model shows a 6 mm/yr velocity of the MF on Profile E, which agrees with the stream offset data of 6 mm/yr (Schwartz et al., 1979).

Some results of the model cannot match with previous studies. The plate motion between the NA and CA is decreasing from 14 mm/yr (Profile E; Figure 4.1) in eastern

Guatemala to 10 mm/yr (Profile C; Figure 4.2) in central Guatemala and 3.5 mm/yr (Profile W; Figure 4.3) in western Guatemala. While, in previous GPS studies, the slip rate of the PMFS decreasing from 16-20 mm/yr in eastern Guatemala (Lyon-Caen et al., 2006; Franco et al., 2012; Ellis et al., 2019), to 12-16 mm/yr (Lyon-Caen et al., 2006; Franco et al., 2012; Ellis et al., 2019) in central Guatemala and 3-5 mm/yr (Franco et al., 2012; Ellis et al., 2019) in western Guatemala. Those differences between the GPS data and our model results may due to the 2D model limitation that cannot capture the grabens. There are three grabens in our model area (the Guatemala City graben; the Ipala graben; the Honduras depression), which could be weakening the graben areas and release more slip rate on the CA. This could be modeled in the 3D model in future studies.

Compare with Previous studies, we included more faults. Therefore, some new information may help to understand the strain partitioning. The degree of strain partitioned on the MF calculated by Franco et al. (2012) and Ellis et al. (2019) are 13 and 18 mm/yr respectively, which is doubled the stream offset data (6 mm/yr) and our model result. The main difference is we introduced more faults in this new FE model, while their 13-18 mm / yr velocity on the MF obtained from inversion based on only one or two faults. For the PF, we also have southern PF in our model, which accommodates about same strain as the northern PF (~3 mm/yr). In addition, the active of JOF (Schwartz et al., 1979) and including the IF (Guzman-Speziale, 2010) accommodate ~3 mm/yr. Therefore, the results of the new FEA model with increased faults are release 6 mm/yr velocity on MF. This phenomenon concludes that since each active fault is assigned a certain strain, an accurate selection of the faults introduced in the model is crucial.

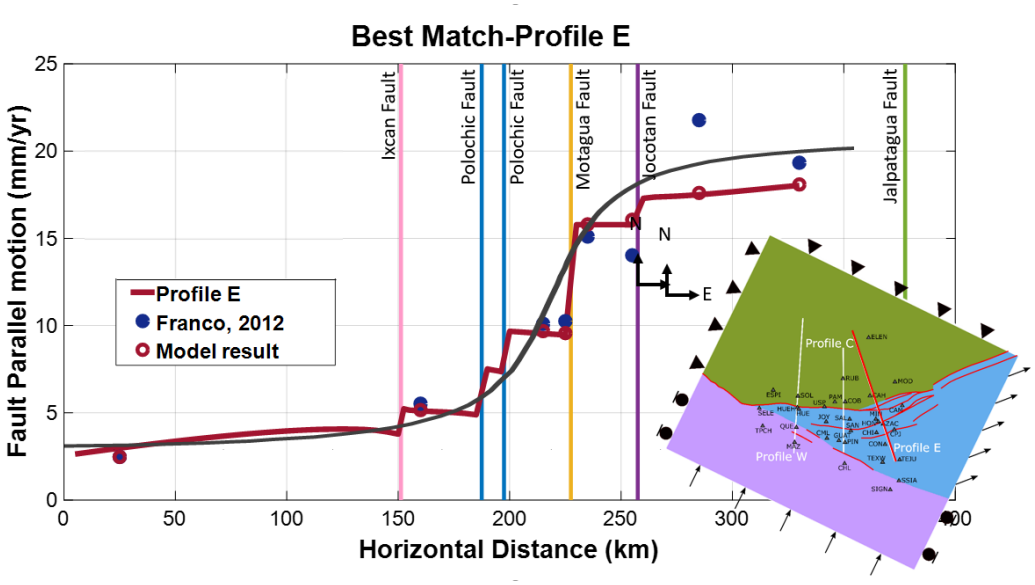

Figure 4.1 The model results of velocity change along profile E based on the best-fit model. The dark red line represents profile E of model results. The grey line represents profile E that estimates from several GPS data in Franco et al. (2012).

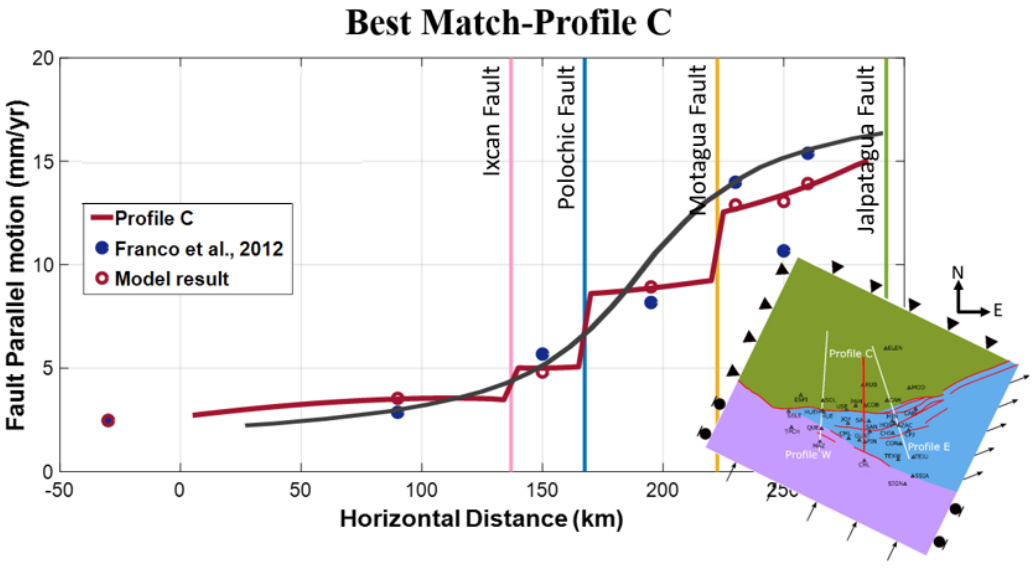

Figure 4.2 The model results of velocity change along profile C based on the best-fit model. The dark red line represents the profile C of model results. The grey line represents the profile C that estimates from several GPS data in Franco et al. (2012).

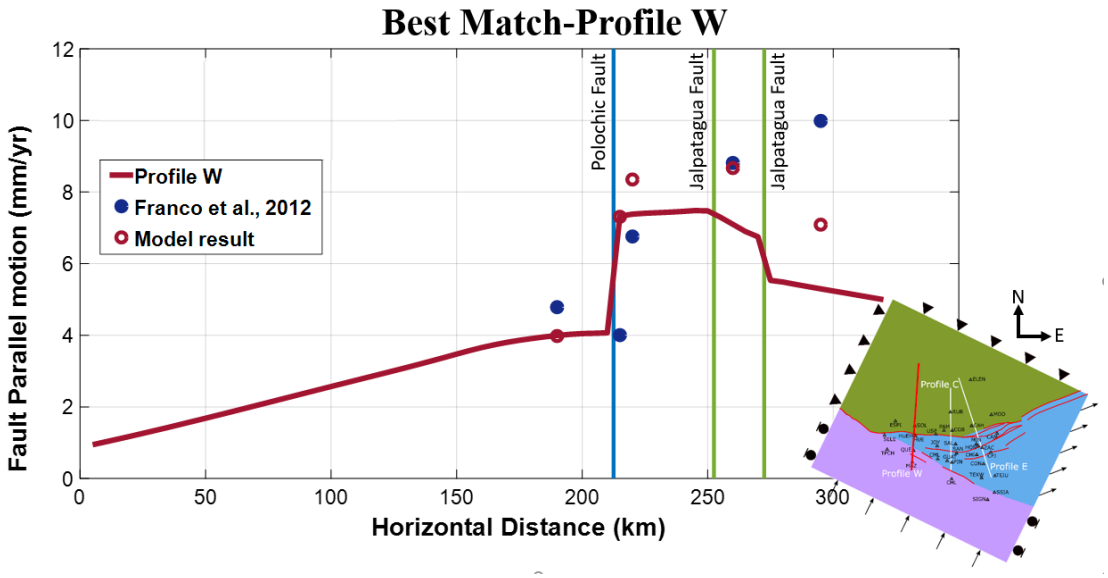

Figure 4.3 The model results of velocity change along profile W based on the best-fit model. The dark red line represents the profile W of model results.

4.3. THE IMPROVEMENTS FROM PROPERTY TESTS

The vector plot shows the differences between the GPS data and the model results in orientation and magnitude. We are using a χ^2 approach from He et al. (2013) to show how differences changed with the testing of properties. The χ^2 that calculate from the base model is 7.9 while from the best-fit model is 3.1. This phenomenon indicates that our research has greatly improved the kinematics of PMFS. While, the obvious differences occur along the JF (Figure 4.4). Even though we have lowered the coupling, based on the current results, there is still a need to be more influenced by the Caribbean plate. This problem could be affected by the uncertainty of the JF, such as the geometry, rheology, or other properties that are not been observed or tested in the 2D model. The area along the JF has consistently caused problems when matching with GPS data (Rodriguez et al., 2009 and Ellis et al., 2019).

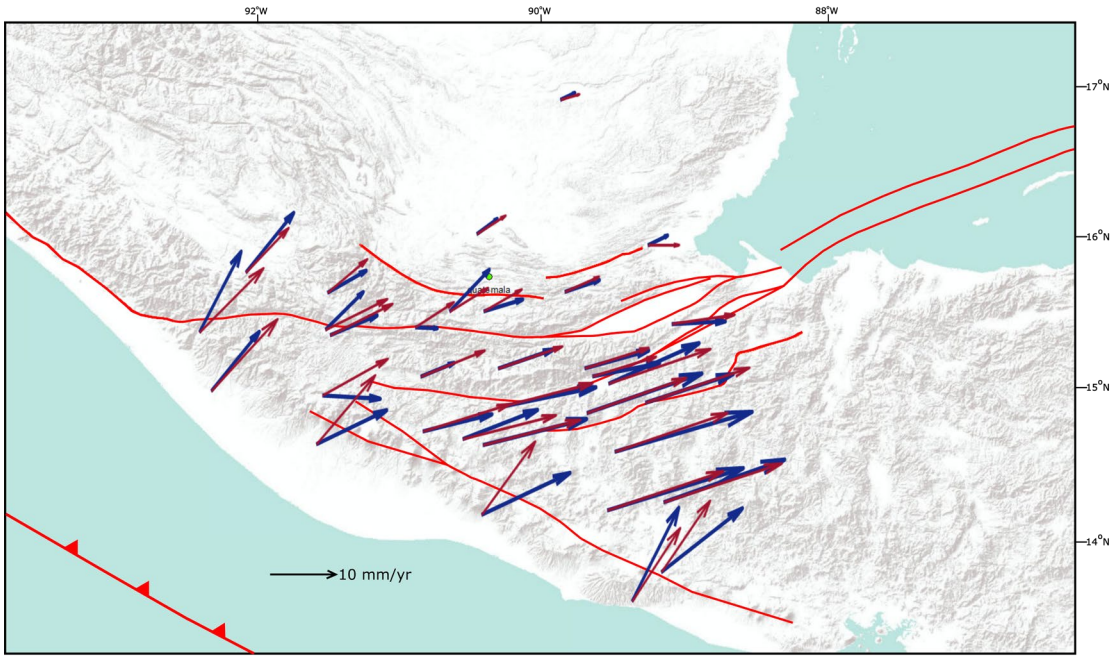

Figure 4.4 The vector plot based on the best-fit model.

4.4. STRAIN FIELD

In Figure 4.5, 4.6, 4.7, and 4.8, axis are principal strain orientations. Orange axis represent contraction and green axis represent dilation. When the strain field shows dilation, it may indicate that the stress decreases in the horizontal direction, and the direction of σ1 will be vertical. In this situation, normal faults may occur. In contrast, when the strain field shows contraction, it may indicate that the direction of σ1 will be horizontal. Therefore, reverse faults may occur. This is a quantitatively conclude about the state of stress without modelling it. With the 2D kinematic model and observed deformation, we can only quantify strain. 3D model and more other information needed for stress studies.

The orientations and relative magnitudes of the principal strain field in those areas are compared with the distribution and appearance of faults observed in geological maps.

In many areas, the results of our model are consistent with the results of geological observations. To the north of the Polochic Fault (Figure 4.5), several reverse faults show near the Cuchumatanes highs with NW-SE orientation (Authemayou et al., 2012). In the same area, the strain field of the model result shows contraction at the direction of NE-SW. Some normal faults appear around the north segment of the Jocotan Fault (Figure 4.6), strike direction is nearly N-S. The model result formed a dilation strain field in nearly W-E. In addition, between the Motagua fault and the Jalpatagua fault (Figure 4.7), in the wedge area, many N-S oriented normal faults appears. The strain field of the model results accurately matches with the indication by showing dilation.

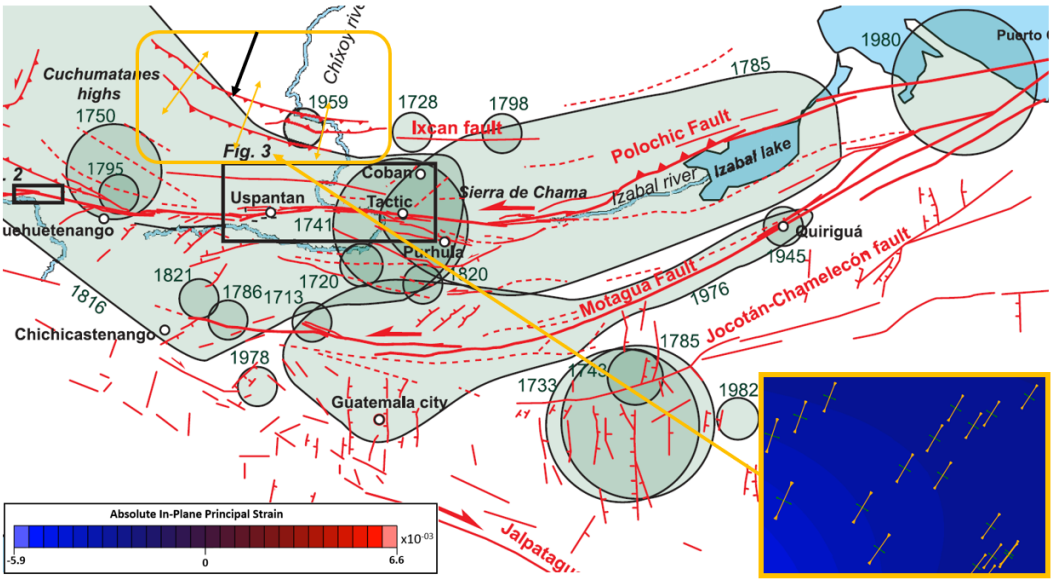

Figure 4.5 Strain fields of model results compare with the fault type to the north of the PF (Authemayou et al., 2012).

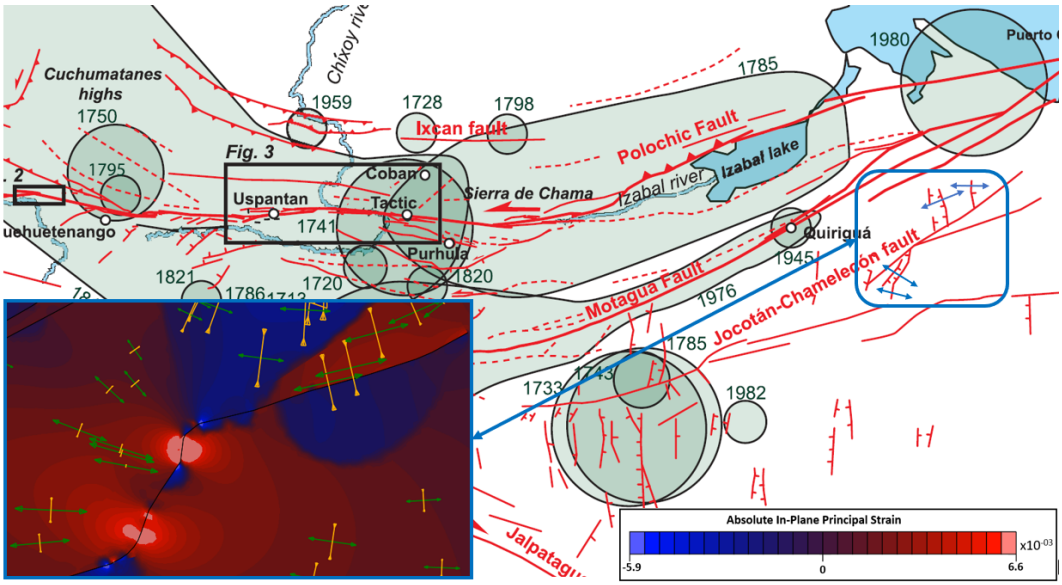

Figure 4.6 Strain fields of model results compare with the fault type in the northern part of the JOF (Authemayou et al., 2012).

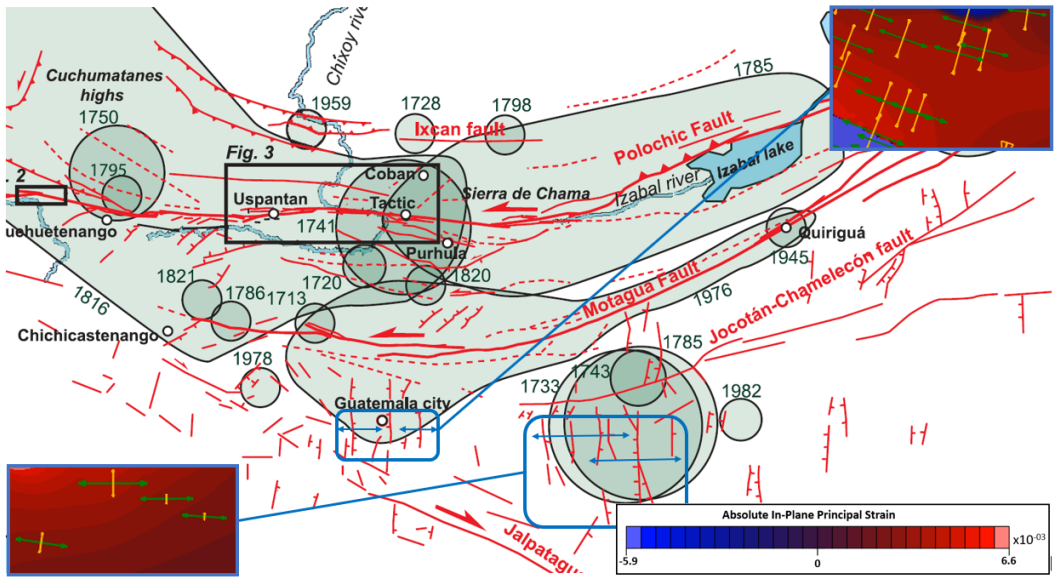

Figure 4.7 Strain fields of model results compare with the fault type in the Guatemala City Graben and Ipala Graben (Authemayou et al., 2012).

There are still some cases that differ from actual measurements. For example, between the Polochic and Motagua faults (Figure 4.8), some normal faults with NE-SW direction are mapped in published maps. While in the model, the principal strain field shows contraction. The vector plot also shows an incongruity with the GPS data around this area. This discrepancy may also be caused by the knowledge gap of geometry.

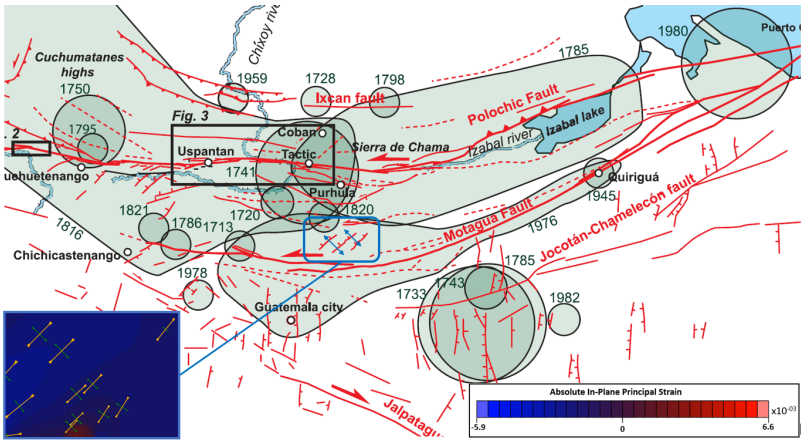

Figure 4.8 Strain fields of model results compare with the fault type between the PF and the MF (Authemayou et al., 2012).

5. CONCLUSION

This study simulates the sinistral transform PMFS, testing geometries and properties, and calibrating with GPS data. From the comparison of model results, the best-fit model which reproduces the GPS data are derived. Model results of the best-fit model investigate the fault system in detail in several ways, including velocity profiles, vector plots, and strain fields.

The key finding in this study is that the fault system is not a simple structure with one or two faults as indicated by the GPS studies. This study shows (Figure 5.1), with including all the major faults, the PMFS is a plate boundary that partitions strain. From our model results, 13% of the total relative motion accommodate on the IF, 18% accommodate on both northern PF and southern PF, 40% on the MF, and 11% on the JOF. Therefore, the plate boundary combined accumulation on those faults, not a simple structure.

Another key finding is from the Chi-square. For the best-fit model, the overall χ^2=3.1, while when we specifically divided data into each block, results are significantly different. The χ^2=1.5 on the CA, 3.6 on the NA, and 9.6 on the forearc sliver. We have a bad fit on forearc sliver while we have a perfect fit on the CA and nearly fit at the NA. The plate boundary fault system is a complex tectonic system, the strike slip tectonics are decoupled from the motion of forearc sliver. This model can predict on in the NA and CA, while cannot predict what is going on in the forearc sliver. More research is necessary for the forearc sliver.

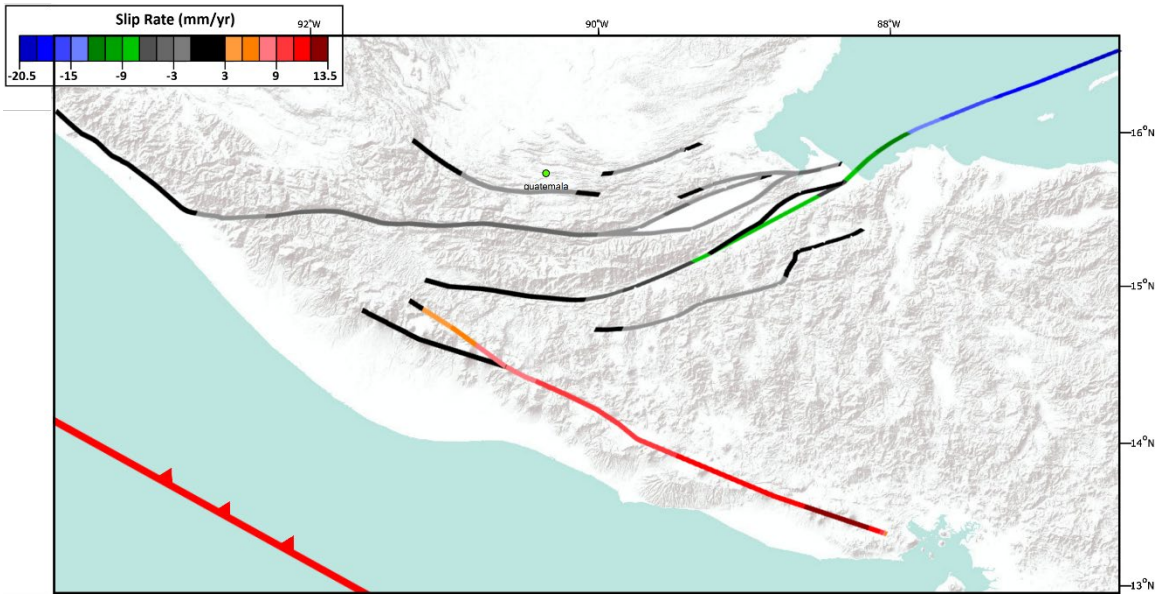

Figure 5.1 The detailed slip rate from the best-fit model.

BIBLIOGRAPHY

Alonso‐Henar, J., Schreurs, G., Martinez‐Díaz, J. J., Álvarez‐Gómez, J. A., & Villamor, P. (2015). Neotectonic development of the El Salvador Fault Zone and implications for deformation in the Central America Volcanic Arc: Insights from 4‐D analog modeling experiments. *Tectonics, 34*(1), 133-151.

Álvarez‐Gómez, J. A., Meijer, P. T., Martínez‐Díaz, J. J., & Capote, R. (2008). Constraints from finite element modeling on the active tectonics of northern Central America and the Middle America Trench. *Tectonics, 27*(1).

Ambraseys, N. N. (1970). Some characteristic features of the Anatolian fault zone. *Tectonophysics*, *9*(2-3), 143-165.

Authemayou, C., Brocard, G., Teyssier, C., Suski, B., Cosenza, B., Morán‐Ical, S., ... & Holliger, K. (2012). Quaternary seismo‐tectonic activity of the Polochic Fault, Guatemala. *Journal of Geophysical Research: Solid Earth, 117*(B7).

Baer, G., Sandwell, D., Williams, S., Bock, Y., & Shamir, G. (1999). Coseismic deformation associated with the November 1995, Mw= 7.1 Nuweiba earthquake, Gulf of Elat (Aqaba), detected by synthetic aperture radar interferometry. *Journal of Geophysical Research: Solid Earth*, *104*(B11), 25221-25232.

Barka, A. A. (1992). The north Anatolian fault zone. In *Annales tectonicae* (Vol. 6, No. Suppl, pp. 164-195).

Barka, A. (1996). Slip distribution along the North Anatolian fault associated with the large earthquakes of the period 1939 to 1967. *Bulletin of the Seismological Society of America, 86*(5), 1238-1254.

Bartole, R., Lodolo, E., Obrist-Farner, J., & Morelli, D. (2019). Sedimentary architecture, structural setting, and Late Cenozoic depocentre migration of an asymmetric transtensional basin: Lake Izabal, eastern Guatemala. *Tectonophysics*, *750*, 419-433.

Bennett, R. A., Rodi, W., & Reilinger, R. E. (1996). Global Positioning System constraints on fault slip rates in southern California and northern Baja, Mexico. *Journal of Geophysical Research: Solid Earth*, *101*(B10), 21943-21960.

Burkart, B. (1978). Offset across the Polochic fault of Guatemala and Chiapas, Mexico. *Geology, 6*(6), 328-332.

Byerlee, J. (1978). The friction of rocks. In *Rock friction and earthquake prediction* (pp. 615-626). Birkhäuser, Basel.

Carpenter, B. M., Saffer, D. M., & Marone, C. (2015). Frictional properties of the active San Andreas Fault at SAFOD: Implications for fault strength and slip behavior. *Journal of Geophysical Research: Solid Earth*, *120*(7), 5273-5289.

Correa-Mora, F., DeMets, C., Alvarado, D., Turner, H. L., Mattioli, G., Hernandez, D., ... & Tenorio, C. (2009). GPS-derived coupling estimates for the Central America subduction zone and volcanic arc faults: El Salvador, Honduras and Nicaragua. *Geophysical Journal International, 179*(3), 1279-1291.

DeMets, C. (2001). A new estimate for present-day Cocos-Caribbean plate motion: Implications for slip along the Central American volcanic arc. *Geophysical research letters, 28*(21), 4043-4046.

De Pascale, G. P., & Langridge, R. M. (2012). New on-fault evidence for a great earthquake in AD 1717, central Alpine fault, New Zealand. *Geology*, *40*(9), 791-794.

Ellis, A., DeMets, C., Briole, P., Cosenza, B., Flores, O., Graham, S. E., ... & Lord, N. (2018). GPS constraints on deformation in northern Central America from 1999 to 2017, Part 1–Time-dependent modelling of large regional earthquakes and their post-seismic effects. *Geophysical Journal International*, *214*(3), 2177-2194.

Ellis, A., DeMets, C., McCaffrey, R., Briole, P., Cosenza Muralles, B., Flores, O., ... & Lord, N. (2019). GPS constraints on deformation in northern Central America from 1999 to 2017, Part 2: Block rotations and fault slip rates, fault locking and distributed deformation. *Geophysical Journal International*, *218*(2), 729-754.

Ferrari, L., Pasquare, G., & Zilioli, E. (1994, December). Kinematics and seismotectonics of a segment of the North America-Caribbean plate boundary: a remote sensing and field study of the Jocotan fault system in Guatemala. In *Geology from Space* (Vol. 2320, pp. 55-64). International Society for Optics and Photonics.

Fialko, Y. (2006). Interseismic strain accumulation and the earthquake potential on the southern San Andreas fault system. *Nature*, *441*(7096), 968.

Fialko, Y., Simons, M., & Agnew, D. (2001). The complete (3-D) surface displacement field in the epicentral area of the 1999 Mw7. 1 Hector Mine earthquake, California, from space geodetic observations. *Geophysical research letters*, *28*(16), 3063-3066.

Fialko, Y., Sandwell, D., Agnew, D., Simons, M., Shearer, P., & Minster, B. (2002). Deformation on nearby faults induced by the 1999 Hector Mine earthquake. *Science*, *297*(5588), 1858-1862. DOI: 10.1126/science.1074671

Franco, A., Lasserre, C., Lyon-Caen, H., Kostoglodov, V., Molina, E., Guzman-Speziale, M., ... & Barrier, E. (2012). Fault kinematics in northern Central America and coupling along the subduction interface of the Cocos Plate, from GPS data in Chiapas (Mexico), Guatemala and El Salvador. *Geophysical Journal International*, *189*(3), 1223-1236.

Garibaldi, N., Tikoff, B., & Hernández, W. (2016). Neotectonic deformation within an extensional stepover in El Salvador magmatic arc, Central America: Implication for the interaction of arc magmatism and deformation. *Tectonophysics*, *693*, 327-339.

Gomez, F., Karam, G., Khawlie, M., McClusky, S., Vernant, P., Reilinger, R., ... & Barazangi, M. (2007). Global Positioning System measurements of strain accumulation and slip transfer through the restraining bend along the Dead Sea fault system in Lebanon. *Geophysical Journal International*, *168*(3), 1021-1028.

Guzmán-Speziale, M. (2010). Beyond the Motagua and Polochic faults: Active strike-slip faulting along the western North America–Caribbean plate boundary zone. *Tectonophysics*, *496*(1-4), 17-27.

Hamiel, Y., Masson, F., Piatibratova, O., & Mizrahi, Y. (2018). GPS measurements of crustal deformation across the southern Arava Valley section of the Dead Sea Fault and implications to regional seismic hazard assessment. *Tectonophysics*, *724*, 171-178.

Hauksson, E., Jones, L. M., Hutton, K., & Eberhart-Phillips, D. (1993). The 1992 Landers earthquake sequence: Seismological observations. *Journal of Geophysical Research: Solid Earth, 98*(B11), 19835-19858.

He, J., Lu, S., & Wang, W. (2013). Three-dimensional mechanical modeling of the GPS velocity field around the northeastern Tibetan plateau and surrounding regions. *Tectonophysics*, *584*, 257-266.

Hussain, E., Hooper, A., Wright, T. J., Walters, R. J., & Bekaert, D. P. (2016). Interseismic strain accumulation across the central North Anatolian Fault from iteratively unwrapped InSAR measurements. *Journal of Geophysical Research: Solid Earth*, *121*(12), 9000-9019.

Langridge, R. M., Villamor, P., Basili, R., Almond, P., Martinez-Diaz, J. J., & Canora, C. (2010). Revised slip rates for the Alpine fault at Inchbonnie: Implications for plate boundary kinematics of South Island, New Zealand. *Lithosphere*, *2*(3), 139-152.

Lavallée, Y., Hirose, T., Kendrick, J. E., De Angelis, S., Petrakova, L., Hornby, A. J., & Dingwell, D. B. (2014). A frictional law for volcanic ash gouge. *Earth and Planetary Science Letters*, *400*, 177-183.

Lefevre, M., Klinger, Y., Al-Qaryouti, M., Le Béon, M., & Moumani, K. (2018). Slip deficit and temporal clustering along the Dead Sea fault from paleoseismological investigations. *Scientific reports*, *8*(1), 4511.

Lindsey, E. O., & Fialko, Y. (2013). Geodetic slip rates in the southern San Andreas Fault system: Effects of elastic heterogeneity and fault geometry. *Journal of Geophysical Research: Solid Earth*, *118*(2), 689-697.

Lindsey, E. O., Sahakian, V. J., Fialko, Y., Bock, Y., Barbot, S., & Rockwell, T. K. (2014). Interseismic strain localization in the San Jacinto fault zone. *Pure and Applied Geophysics*, *171*(11), 2937-2954.

Lodolo, E., Menichetti, M., Guzmán-Speziale, M., Giunta, G., & Zanolla, C. (2009). Deep structural setting of the North American-Caribbean plate boundary in eastern Guatemala. *Geofísica internacional, 48*(3), 263-277.

Lyon-Caen, H., Barrier, E., Lasserre, C., Franco, A., Arzu, I., Chiquin, L., ... & Luna, J. (2006). Kinematics of the North American–Caribbean-Cocos plates in Central America from new GPS measurements across the Polochic-Motagua fault system. *Geophysical Research Letters*, *33*(19).

McGill, S., Dergham, S., Barton, K., Berney-Ficklin, T., Grant, D., Hartling, C., ... & Russell, J. (2002). Paleoseismology of the San Andreas fault at Plunge Creek, near San Bernardino, southern California. *Bulletin of the Seismological Society of America*, *92*(7), 2803-2840.

Nabavi, S. T., Alavi, S. A., & Maerten, F. (2018). 2D finite-element elastic models of transtensional pull-apart basins. *Comptes Rendus Geoscience*, *350*(5), 222-230.

Norris, R. J., & Cooper, A. F. (2001). Late Quaternary slip rates and slip partitioning on the Alpine Fault, New Zealand. *Journal of Structural Geology*, *23*(2-3), 507-520.

Olcese, O., Moreno, R., & Ibarra, F. (1977). The Guatemala earthquake disaster of 1976: A review of its effects and of the contribution of the United Nations family. *UN Development Program. July 1977. sl GT*.

Plafker, G. (1976). Tectonic aspects of the Guatemala earthquake of 4 February 1976. *Science*, *193*(4259), 1201-1208.

Ratschbacher, L., Franz, L., Min, M., Bachmann, R., Martens, U., Stanek, K., ... & López-Martínez, M. (2009). The North American-Caribbean plate boundary in Mexico-Guatemala-Honduras. *Geological Society, London, Special Publications, 328*(1), 219-293.

Rodriguez, M., DeMets, C., Rogers, R., Tenorio, C., & Hernandez, D. (2009). A GPS and modelling study of deformation in northern Central America. *Geophysical Journal International*, *178*(3), 1733-1754.

Rosenberg, C. L., & Handy, M. R. (2005). Experimental deformation of partially melted granite revisited: implications for the continental crust. *Journal of metamorphic Geology*, *23*(1), 19-28.

Schwartz, D. P., Cluff, L. S., & Donnelly, T. W. (1979). Quaternary faulting along the Caribbean-North American plate boundary in Central America. *Tectonophysics*, *52*(1-4), 431-445.

Stein, R. S., Barka, A. A., & Dieterich, J. H. (1997). Progressive failure on the North Anatolian fault since 1939 by earthquake stress triggering. *Geophysical Journal International*, *128*(3), 594-604.

Sutherland, R., Eberhart-Phillips, D., Harris, R. A., Stern, T., Beavan, J., Ellis, S., ... & Townend, J. (2007). Do great earthquakes occur on the Alpine fault in central South Island, New Zealand?. *GEOPHYSICAL MONOGRAPH-AMERICAN GEOPHYSICAL UNION*, *175*, 237.

Szeliga, W., Bilham, R., Kakar, D. M., & Lodi, S. H. (2012). Interseismic strain accumulation along the western boundary of the Indian subcontinent. *Journal of Geophysical Research: Solid Earth*, *117*(B8).

Tymofyeyeva, E., & Fialko, Y. (2018). Geodetic evidence for a blind fault segment at the southern end of the San Jacinto Fault Zone. *Journal of Geophysical Research: Solid Earth*, *123*(1), 878-891.

Wdowinski, S., Bock, Y., Baer, G., Prawirodirdjo, L., Bechor, N., Naaman, S., ... & Melzer, Y. (2004). GPS measurements of current crustal movements along the Dead Sea Fault. *Journal of Geophysical Research: Solid Earth*, *109*(B5).

Wechsler, N., Rockwell, T. K., & Klinger, Y. (2018). Variable slip-rate and slip-per-event on a plate boundary fault: The Dead Sea fault in northern Israel. *Tectonophysics*, *722*, 210-226.

White, R. A. (1984). Catalog of historic seismicity in the vicinity of the Chixoy-Polochic and Motagua faults, Guatemala (No. 84-88). US Geological Survey,.

VITA

Qiaoqi Sun was born and grew up in Tianjin, China. She earned her bachelor's degree in Resources Exploration Engineering from Yangtze University (China) in May 2017. After graduation, she attended the Missouri University of Science and Technology, in Rolla, Missouri for the master's degree. She started her master's program in Geology and Geophysics in August 2017, working with Dr. Andreas Eckert and Dr. Obrist-Farner. She received her Master of Science in Geology and Geophysics from Missouri University of Science and Technology in May 2020.